

Supporting Information

Coupling EC CO₂ reduction on PhC₂Cu-gas diffusion electrode with PEC glycerol oxidation on AuCu/TiO₂HNTAs

Danfeng Liu, Yiwei Zhou, Bingxu Chen, Jian Zhao*

^a Tianjin Key Laboratory of Organic Solar Cells and Photochemical Conversion, School of Chemistry and Chemical Engineering, Tianjin University of Technology, Tianjin 300384, China.

*Email: zjtjbd@hotmail.com; zjtjbd@email.tjut.edu.cn

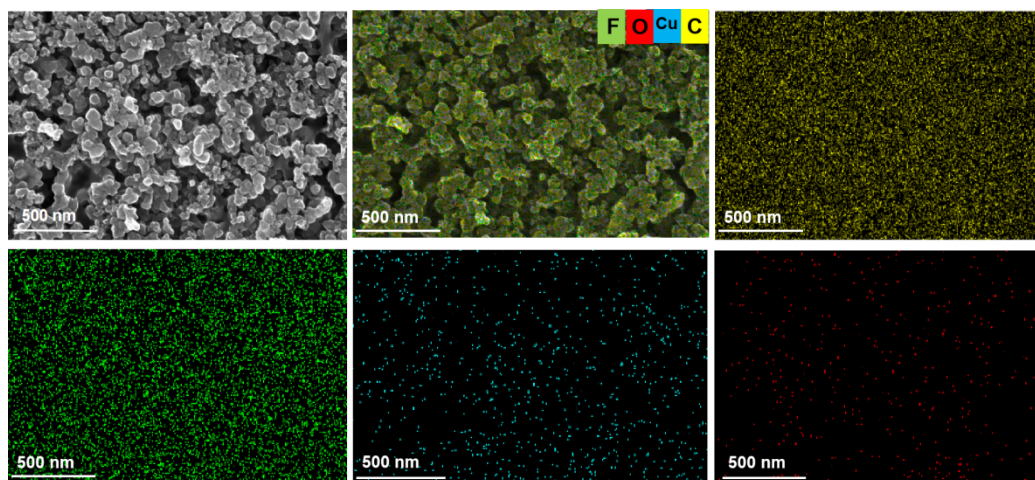


Figure S1. The SEM-EDS of 10 wt% PhC₂Cu-GDE

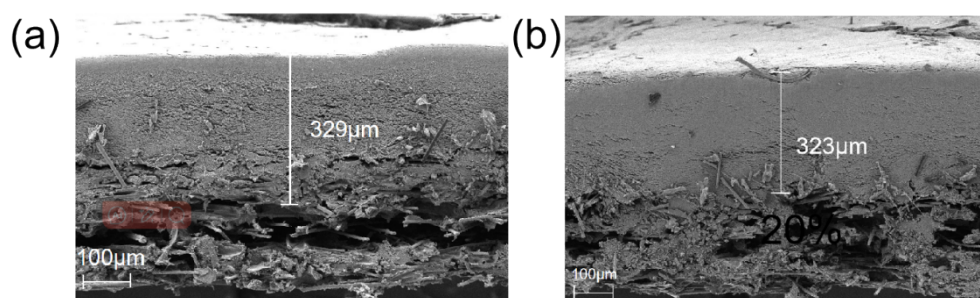


Figure S2. The SEM image for the cross-section of (a) 5% PhC₂Cu-GDE and (b) 20% PhC₂Cu-GDE.

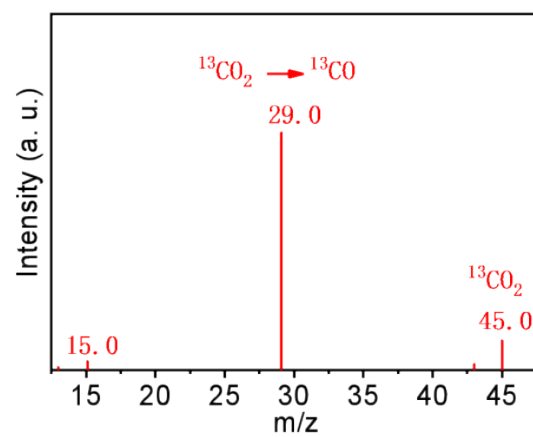


Figure S3. The GC-MS of the gas product after EC $^{13}\text{CO}_2$ RR.

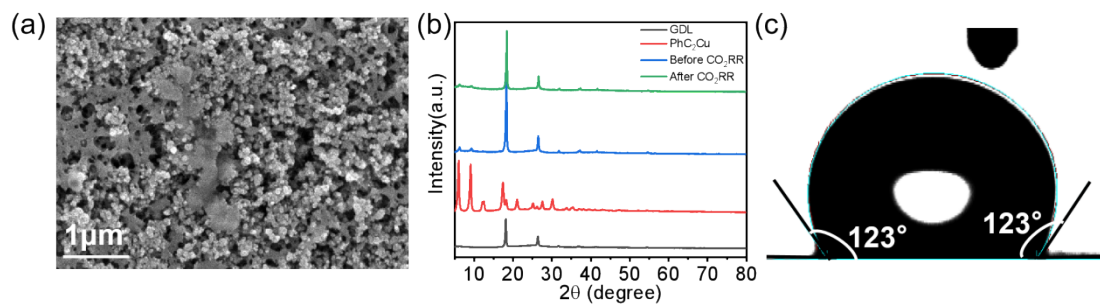


Figure S4. The (a) SEM image (b) XRD pattern and (c) the contact Angle of PhC₂Cu-GDE after EC CO₂RR.

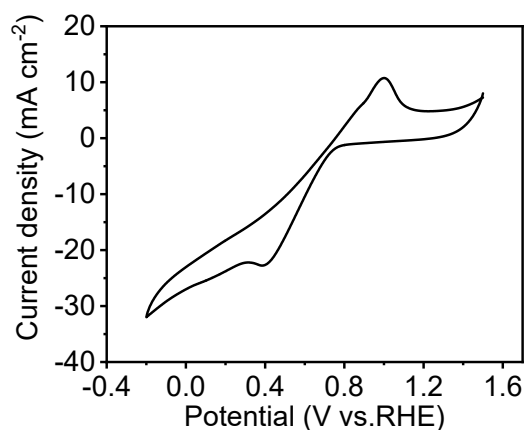


Figure S5. Cyclic voltammetry curve of 10% PhC₂Cu-GDE.

The Cyclic voltammetry curve of the prepared gas diffusion electrode was scanned over a voltage range from -1.2 V to 1.5 V vs. RHE. Figure S2 illustrates the redox-oxidation peak of the PhC₂Cu-GDE gas diffusion electrode and the non-Faradaic current region. 0.80~0.96 V vs. RHE in the non-Faradaic region was selected to conduct cyclic voltammetry (CV) scans at various scan rates, obtaining the cyclic voltammetry curves in Figure S3. Subsequently, the current density ($(j_1-j_2)/2$) at 0.88 V vs. RHE was plotted against the sweep rate, yielding a straight line whose slope represents the double-layer capacitance (Cdl).

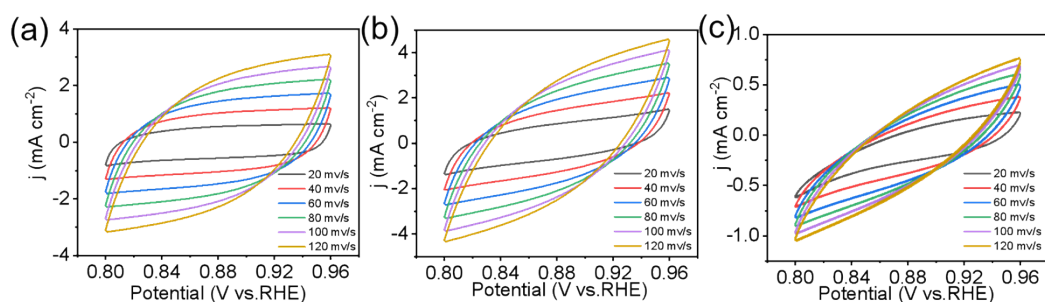


Figure S6. Cyclic voltammetry curves of PhC₂Cu-based GDE at different scanning rates. (a) 5% PhC₂Cu-GDE, (b) 10% PhC₂Cu-GDE, (c) 20% PhC₂Cu-GDE.

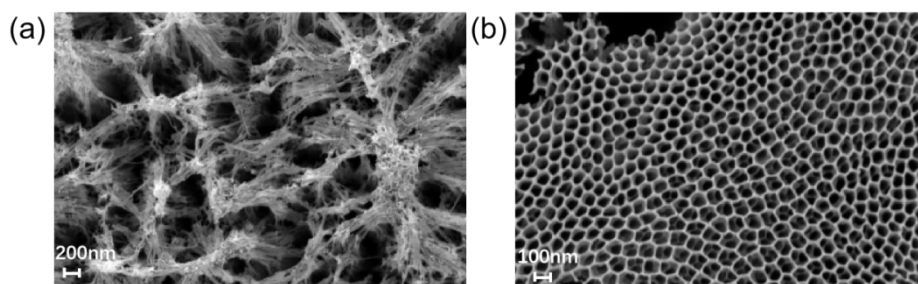


Figure S7. SEM images of TiO_2HNTAs after the second anodization step. (a indicates the side facing the platinum electrode surface and b indicates the side facing away from the platinum electrode surface during the second anodization step)

Scanning Electron Microscopy (SEM) characterization of the surface morphology revealed non-hierarchical and non-ordered nanotube structure for the side directly facing the platinum electrode surface (Figure S4a). For the side facing away from the platinum electrode surface during the second anodization step (Figure S4b), a hierarchical nanotube array structure with a photonic-like layer was observed, noted as TiO_2HNTAs . In our former works, we have proved that TiO_2HNTAs exhibited higher photocatalytic activity than TiO_2 nanotubes without the hierarchical structure, thus following experiments was conducted on the TiO_2HNTAs surface.

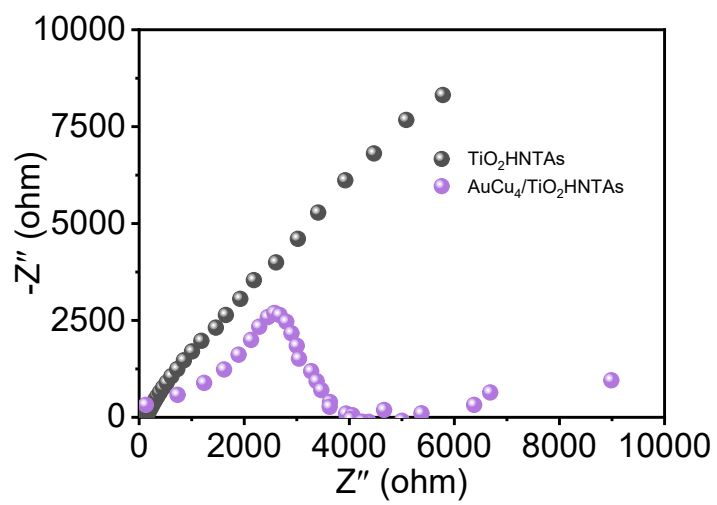


Figure S8. EIS of the TiO₂HNTAs and AuCu₄/TiO₂HNTAs.

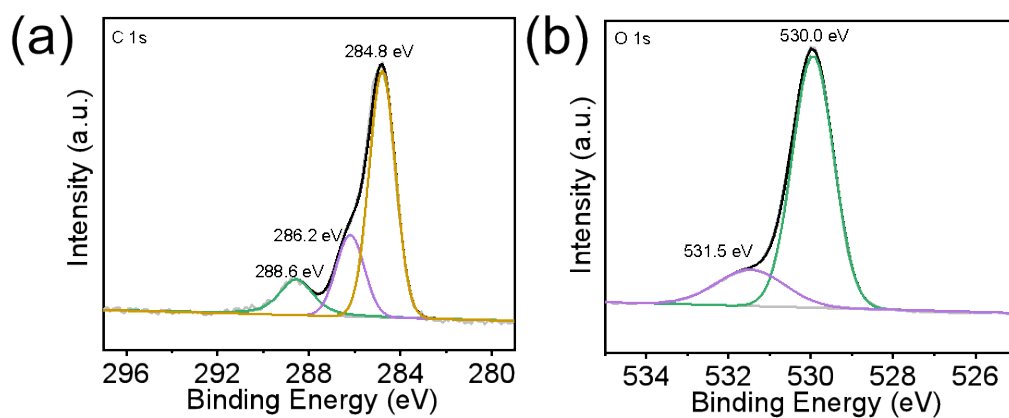


Figure S9. XPS analysis of 0.05 wt% AuCu₄/TiO₂ HNTAs. (a) C 1s and (b) O 1s.

The C1s peak at 284.8 eV was selected as the standard binding energy of C1s (Figure S9a). In the O1s spectrum (Figure S9b), the characteristic peak at 530.0 eV corresponds to the Ti-O-Ti bond in TiO₂.

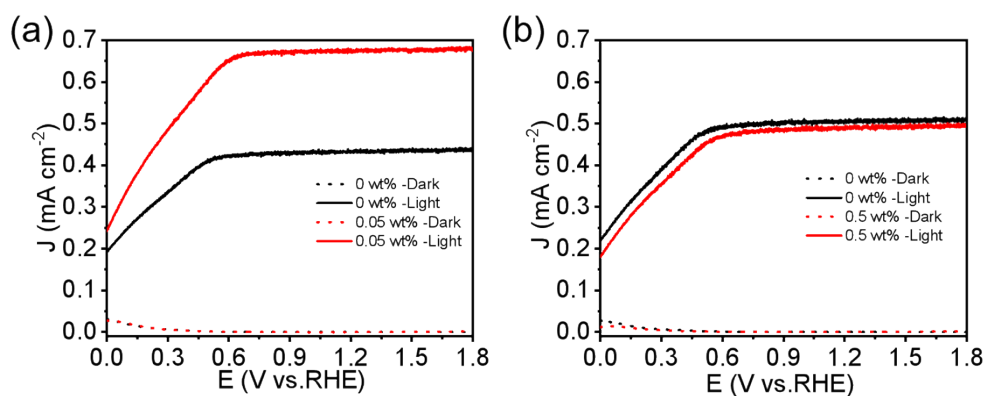


Figure S10. LSV curves of TiO_2HNTAs , (a) 0.05 wt% $\text{Au}_4\text{Cu}/\text{TiO}_2\text{HNTAs}$ and b) 0.5 wt% $\text{Au}_4\text{Cu}/\text{TiO}_2\text{HNTAs}$ under light and in the dark conditions with 0.01 M glycerol (GLY). 0.5 M Na_2SO_4 , AM 1.5G, 120 mW/cm^2 .

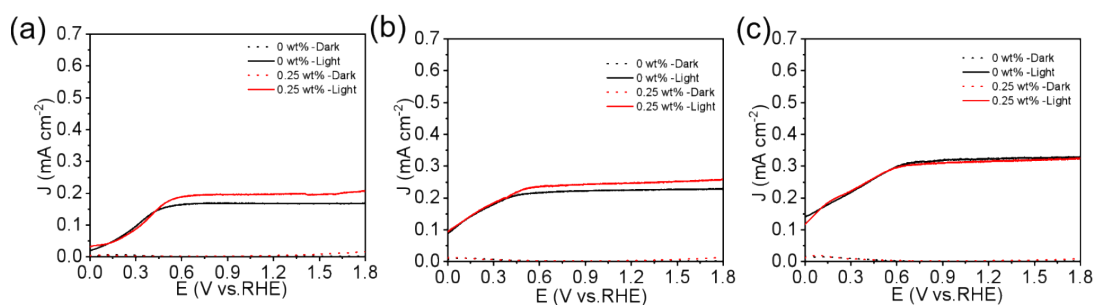


Figure S11. LSV curves of TiO_2HNTAs , 0.25 wt% $\text{Au}_4\text{Cu}/\text{TiO}_2\text{HNTAs}$ under light and in the dark. (a) without glycerol, (b) with 0.01 M glycerol, (c) with 0.1M glycerol. 0.5 M Na_2SO_4 , AM 1.5G, 120 mW/cm^2 .

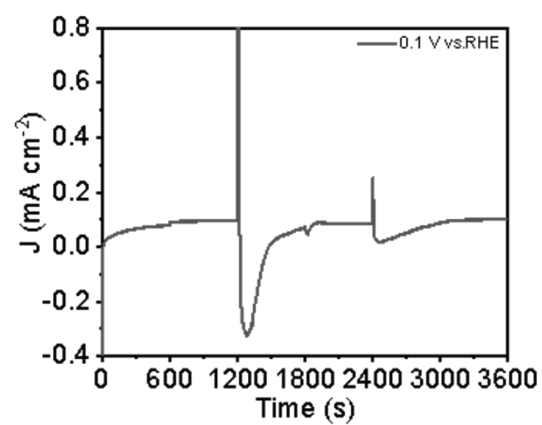


Figure S12. I-t curve of glycerol (0.01 M) oxidation on AuCu₄/TiO₂HNTAs at 0.1 V vs. RHE.

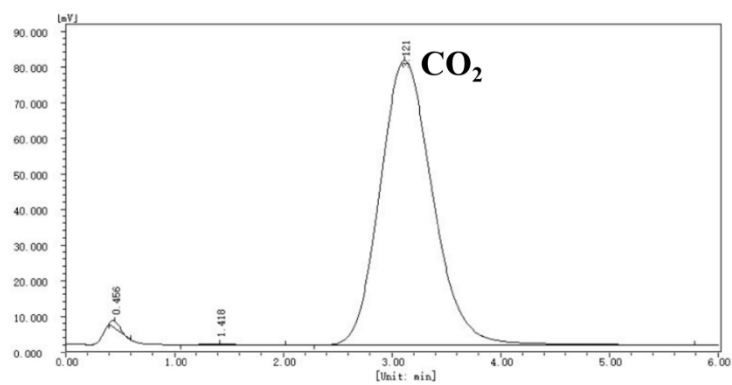


Figure S13. GC spectra of the gas product for glycerol oxidation on AuCu₄/TiO₂HNTAs after 20 min at 0.1 V vs. RHE.

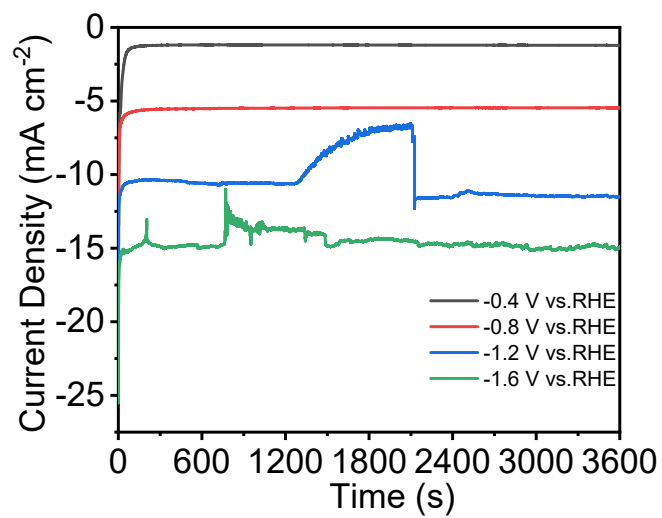


Figure S14. I-t curves for CO₂RR at different potentials after coupling with PEC glycerol oxidation.

Faradic efficiencies of gas products:

$$FE_{\text{gas product}} = \frac{N_{\text{gas}}}{N_{\text{total}}} \times 100\% = \frac{X_0 * n * N_A * e^{-}(\text{transfer number})}{\frac{I_0 * t}{e}} \times 100\%$$

Where n is the number of reaction moles, X_0 is the amount of gas detected by GC, N_A is the Avogadro constant of 6.02×10^{23} , I_0 is the instantaneous current, t is the filling time for sample loop.

The volume of the sample loop (V_0) for gas products in our online GC is 2 cm^3 and the flow rate of the gas is $v = 20 \text{ cm}^3 / \text{min}$. Then, the time required to fill the sample loop is:

$$t = \frac{V_0}{v} = \frac{2 \text{ cm}^3}{20 \text{ cm}^3/\text{min}} = 0.1 \text{ min} = 6 \text{ s}$$

According to the ideal gas law, under ambient temperature of $26 \text{ }^\circ\text{C}$, the amount of gas in each vial ($V_0 = 1 \text{ cm}^3$) is:

$$n = \frac{P \times V_0}{R \times T} = \frac{1.013 \times 10^5 \text{ Pa} \times 2 \times 10^{-6} \text{ m}^3}{8.314 \text{ J} \cdot \text{K}^{-1} \cdot \text{mol}^{-1} \times 299.15 \text{ K}} = 8.146 \times 10^{-5} \text{ mol}$$

The number of electrons required to form H_2 , CO , CH_4 , C_2H_4 and C_2H_6 is 2, 2, 8, 12, and 14, respectively. Taking the Faraday efficiency of CO as an example, assume that the amount of CO detected by GC (X_0) is 6068.89 ppm. The number of electrons required to produce CO is:

$$N_{\text{CO}} = x_0 \times n \times N_A \times 2e = 6068.89 \times 10^{-6} \times 8.146 \times 10^{-5} \times 6.02 \times 10^{23} \text{ mol}^{-1} \times 2e = 5.952 \times 10^{17} e$$

If the current $I_0 = 17.18 \text{ mA}$, then

$$N_{\text{total}} = \frac{I_0 \times t}{e} = \frac{17.18 \times 10^{-3} \text{ A} \times 6 \text{ s}}{1.602 \times 10^{-19} \text{ C/e}} = 6.434 \times 10^{17} e$$

Therefore, the Faraday efficiency of CO is:

$$N_{\text{CO}} = \frac{N_{\text{CO}}}{N_{\text{total}}} \times 100\% = \frac{5.952 \times 10^{17}}{6.434 \times 10^{17}} \times 100\% = 86.91\%$$